nature geoscience

Article

https://doi.org/10.1038/s41561-024-01532-z

Upwelling of melt-depleted mantle under Iceland

Received: 23 November 2023

Accepted: 2 August 2024

Published online: 29 August 2024

Check for updates

A. Sanfilippo[1,2] ✉, A. Stracke[3] ✉, F. Genske[3], S. Scarani[1], M. Cuffaro[4], V. Basch[1,2], G. Borghini[5], D. Brunelli[4,6], C. Ferrando[1,7], A. A. Peyve[8] & M. Ligi[9]

Seafloor anomalies along mid-ocean ridges with exceptionally thick and compositionally distinct basaltic crust, for example, at Iceland, suggest that the underlying mantle is hotter and chemically different from the adjacent subridge mantle. Here we present hafnium and neodymium isotope ratios of peridotites from the Charlie Gibbs Transform Zone, which is located at the southern end of the Reykjanes Ridge south-west of Iceland. These peridotites are strongly depleted in incompatible elements with extremely high hafnium isotope ratios, suggesting that they had already melted to a large extent before being incorporated into the plume, at least 1 billion years ago, and thereby also became less dense. We argue that seismic velocity anomalies, geodynamic models and geochemical affinities of ridge basalts connect the peridotites from the Charlie Gibbs Transform Zone to the 'Iceland plume'. The thermochemical buoyancy of the moderately hot Iceland plume, but also that of other plumes worldwide, may therefore be strongly influenced by composition. Variable peridotite depletion along the rising Iceland plume could also cause the transient, density-driven pulses in plume flux, which have formed the V-shaped Reykjanes Ridge south of Iceland. Overall, expansion of a ridge-centred plume along adjacent ridges and melting of heterogeneous plume material explains the topographic swell, the seismic anomaly and the formation of V-shaped ridges, as well as the regional distribution of basalts with Icelandic affinity.

Abyssal peridotites are mantle rocks from which melt has been extracted during one or more previous melting events, primarily under mid-ocean ridges. Most abyssal peridotites are therefore incompatible element (ICE) depleted, and clinopyroxene (cpx)-poor peridotites or harzburgites (<5 wt% cpx) with high Sm/Nd and Lu/Hf ratios. Over time, such residual peridotites develop extremely high Nd and Hf isotope ratios, much higher than those observed in mid-ocean ridge basalts (MORBs)[1–3]. The expected high Hf isotope ratios are indeed observed in abyssal peridotites[1–3], but are also found in peridotites from ophiolites, plume-related peridotite xenoliths[1–5] and peridotites from the subcontinental lithospheric mantle (SCLM)[6] (Fig. 1). Yet, these so-called ultradepleted Hf isotope ratios are often not correlated with high Nd isotope ratios, implying that the majority of peridotites from the oceans and continents are not strictly residual, but have reacted with migrating or stalled melts at some point during their evolution[2,3,7–12].

[1]Dipartimento di Scienze della Terra e dell'Ambiente, Università di Pavia, Pavia, Italy. [2]Istituto di Geoscienze e Georisorse CNR, Pavia, Italy. [3]Institut für Mineralogie, Universität Münster, Münster, Germany. [4]Istituto di Geologia Ambientale e Geoingegneria CNR, Roma, Italy. [5]Dipartimento di Scienze della Terra, Università degli Studi di Milano, Milan, Italy. [6]Dipartimento di Scienze Chimiche e Geologiche, Università di Modena e Reggio Emilia, Modena, Italy. [7]Dipartimento di Scienze della Terra, dell'Ambiente e della Vita, Università di Genova, Genova, Italy. [8]Geological Institute, Russian Academy of Sciences, Moscow, Russia. [9]Istituto di Scienze Marine CNR, Bologna, Italy. ✉e-mail: alessio.sanfilippo@unipv.it; astra_01@uni-muenster.de

https://doi.org/10.1038/s41561-024-01532-z

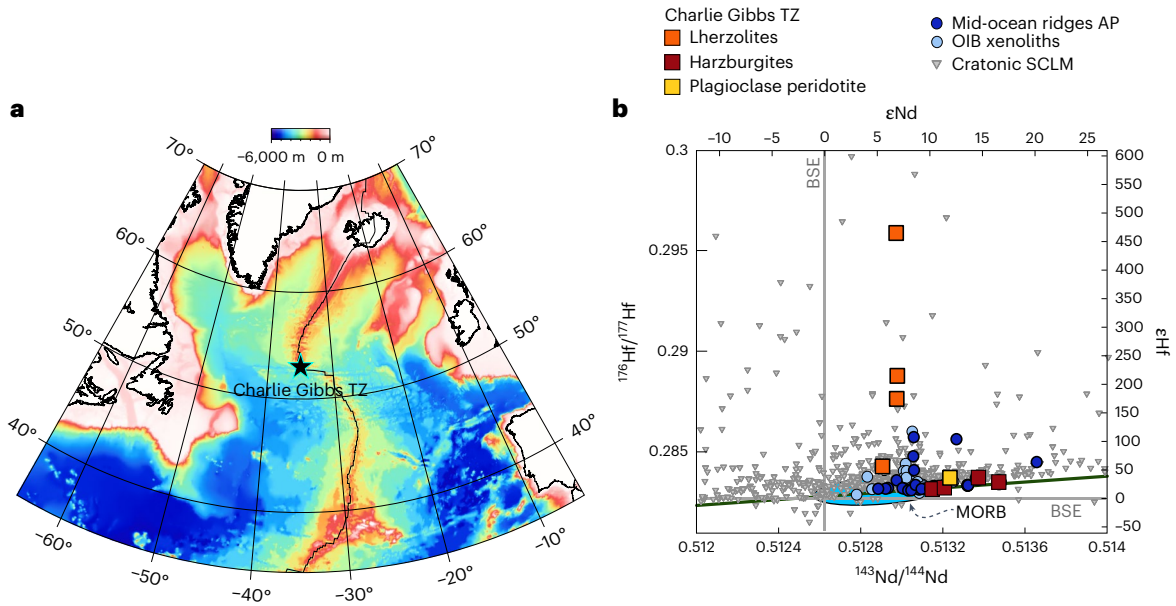

Fig. 1 | Location of Charlie Gibbs TZ and global compilation of Hf–Nd isotopes in mantle peridotites. a, Bathymetry of the northern Atlantic from the General Bathymetric Chart of the Oceans (GEBCO) 2023 Grid (https://doi.org/10.5285/f98b053b-0cbc-6c23-e053-6c86abc0af7b; GEBCO Compilation Group) showing the location of the Charlie Gibbs transform zone (TZ) (star). **b**, A diagram showing the Hf and Nd isotope ratios of cpx from Charlie Gibbs peridotites (error bars are smaller than the data points) compared with cpx from other abyssal peridotites (AP)[1–3] and peridotite xenoliths from ocean island basalts (OIB)[30]. Also shown are cpx and whole-rock data of cratonic SCLM (see compilation in ref. 6). The field of Atlantic MORB erupted between the Azores (40° N) and Iceland (62° N) is also indicated (compiled from PetDB, www.earthchem.org/petdb). The grey lines in Fig. 1b denote the Hf and Nd isotope ratios of the bulk silicate Earth (BSE).

Invariably, cpx crystallizes during melt-rock reaction[13,14] and thereby forms 'secondary' lherzolites, which are cpx-rich (~10–20%) peridotites[7,8,10]. The residual peridotites that have been recirculated within the mantle after subridge processing—and now re-melt under mid-ocean ridges and ocean islands after several 10^2–10^3 Ma mantle residence—therefore have variable chemical compositions and density. These diverse peridotites are frequently found in close association on the ocean floor, with a length scale of chemical heterogeneity from 10^{-2} to 10^4 m (refs. 3,10,12). Occasionally, melt-depleted, light peridotites support entire ridge segments, such as the shallow Marion Rise along the Southwest Indian Ridge[15], and thus cause variations in ridge topography.

Here, we report chemical and Hf–Nd isotope data of peridotites collected at the Charlie Gibbs TZ, located at 53° N at the Mid-Atlantic Ridge (MAR). This fracture zone is the southern boundary of the large area of low shear wave velocity that marks the dispersion of the 'Iceland plume'[16–20]. As the peridotites from the Charlie Gibbs TZ are sampled above the area influenced by the Iceland plume, we argue below that they represent the predominant peridotitic part of the Iceland plume and thus provide critical constraints on its composition.

Mantle peridotites from the Charlie Gibbs TZ

The Charlie Gibbs TZ is a multi-fault transform system that offsets the MAR by 380 km at the southern end of the Reykjanes Ridge at 52–53° N (Fig. 1 and Extended Data Figs. 1 and 2). Peridotites were collected during expeditions S50 and V53 on board the R/V A.N. Strakhov and A.S. Vavilov[21]. Detailed petrographical features of the samples are described in Methods and are illustrated in Extended Data Fig. 3.

The investigated peridotites are partly serpentinized harzburgites and lherzolites. The harzburgites contain olivines with high forsterite content ([Mg/(Mg+Fe) mol%] = 91–90), rounded spinels with variable Cr# ([Cr/(Cr + Al) mol%] = 17–32) and rare cpx with high Mg# ([Mg/(Mg + Fe) mol%] = 91–93) and Al_2O_3 contents (5–6 wt%). The cpx from the harzburgite are also strongly depleted in TiO_2, Hf and rare earth elements (REEs) (Fig. 2a,b), and have higher middle-to-heavy REE contents, as well as more pronounced depletions of the light REE (Ce_N/Sm_N = 0.02) and Zr (Zr_N/Nd_N = 0.1–0.2) compared with cpx from the lherzolites (subscript N indicates normalization to bulk silicate Earth[22]). The compositions of the harzburgites thus resemble simple partial melting residues (Extended Data Figs. 4 and 5). Only one of the harzburgites contains plagioclase–pyroxene veins (hereafter referred to as Pl-harzburgite; Extended Data Fig. 3), which crosscut the deformed mantle minerals, indicative of melt impregnation at shallow levels.

In contrast, the lherzolites have very low TiO_2, Zr, Hf and middle-heavy REE contents in cpx (Fig. 2a,b), and high forsterite contents in olivine (91–92 mol%), despite being cpx rich. Plagioclase is absent and cpx occurs as microveins or inter-granular crystals characterized by high Al_2O_3 (5.5 wt%) and Mg# (92–93 mol%). Overall, the cpx in the lherzolites are more depleted in ICE than those in the harzburgites. The lherzolites cannot be mere residues of partial melting however, because (1) spinels appear as interstitial amoeboid grains often aligned along a preferential direction and have low Cr# (18–25) and (2) cpx are mostly inter-granular crystals with high Na_2O contents (up to 0.8 wt%) and enrichments in light REE (Ce_N/Sm_N = 0.2–0.5; Fig. 2b) compared with the harzburgites. This means that spinel and cpx probably crystallized during the reaction between an ICE-depleted protolith and migrating melts. Collectively, the high Na_2O and light REE contents observed in the cpx from the lherzolites indicate that recent reactions with migrating alkaline melts led to crystallization of cpx, and re-enrichment of ICE[7,9,11]. Substantial depletion of the middle-heavy REE, Ti and Y on the other hand, suggests that these rocks were originally more ICE depleted than the harzburgites (Extended Data Figs. 4 and 5).

The Nd and Hf isotope ratios observed in peridotites from the Charlie Gibbs TZ far exceed the variability in MORBs erupted along the MAR from 45°–70° N. The harzburgites have high $^{147}Sm/^{144}Nd$ (0.72–0.94) and $^{143}Nd/^{144}Nd$ (0.5132–0.5136) (εNd of 10.1–16.5); the latter are slightly lower in one Pl-bearing sample (Fig. 2c). The $^{176}Lu/^{177}Hf$ range from 0.12 to 0.22 and are coupled with MORB-like $^{176}Hf/^{177}Hf$ (0.2832–0.2837) (εHf of 16.9–32.3) (Fig. 2c). The lherzolites have low and

https://doi.org/10.1038/s41561-024-01532-z

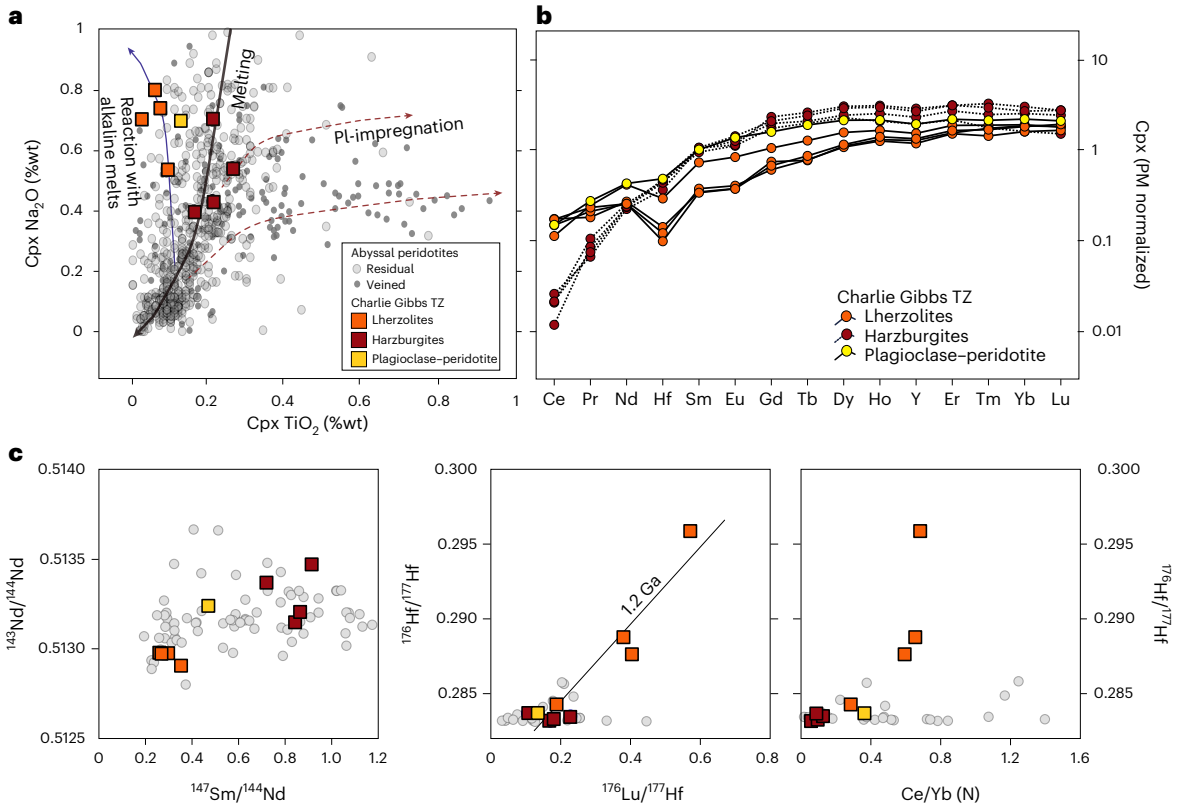

Fig. 2 | Major, trace elements and Nd–Hf isotopes of Charlie Gibbs peridotites. **a**, Covariation in Na_2O and TiO_2 cpx contents of the Charlie Gibbs peridotites. Global abyssal peridotites are shown as grey dots[12]. Schematic trends show how Na_2O and TiO_2 contents in cpx change with progressive partial melting (thick grey line), plagioclase impregnation (red line) and reaction with alkaline melts (blue line)[9,12]. **b**, Primitive mantle (PM)-normalized[22] Hf–Y–REE concentrations of cpx from the peridotites in this study. **c**, Diagrams showing Hf and Nd isotope ratios versus trace element indices of depletion in cpxs from peridotites of the Charlie Gibbs TZ (error bars are smaller than the data points) and global abyssal peridotites (grey dots; data compilation from Fig. 1). Cpxs in residual harzburgites from this study (dark red squares) have low Nd–Hf isotope ratios and ICE-depleted trace element compositions in agreement with their residual character. Cpxs from the lherzolites (orange squares) have very high $^{176}Hf/^{177}Hf$ coupled with low $^{143}Nd/^{144}Nd$, but high Ce/Yb, low $^{147}Sm/^{144}Nd$ and variable $^{176}Lu/^{177}Hf$. These data suggest that these highly depleted peridotites were recently re-enriched with ICEs by melt-rock reactions. Plagioclase harzburgite cpxs (yellow square) have $^{176}Hf/^{177}Hf$ and $^{143}Nd/^{144}Nd$, similar to the residual harzburgites but slightly lower Sm/Nd and higher Ce/Yb as a result of recent interaction with migrating melts.

nearly constant $^{147}Sm/^{144}Nd$ (0.26–0.35) and $^{143}Nd/^{144}Nd$ (0.5129–0.5130) (εNd of 5.4–6.8) (Fig. 2c), while their $^{176}Lu/^{177}Hf$ vary from 0.2 to 0.6 (Fig. 2c). Remarkably, the $^{176}Hf/^{177}Hf$ of the lherzolites range from 0.2843 to 0.2959 (εHf of 53–463). The highest εHf value of 463 is much higher than any previously reported $^{176}Hf/^{177}Hf$ in abyssal peridotites. While the correlation between $^{147}Sm/^{144}Nd$ and $^{176}Lu/^{177}Hf$ (Extended Data Fig. 5) and the low $(Ce/Yb)_N$ (Fig. 2c) in the harzburgites are consistent with a residual origin, the lherzolites have high $^{176}Lu/^{177}Hf$ coupled to low $^{147}Sm/^{144}Nd$ and high $(Ce/Yb)_N$ (Fig. 2c), indicating recent re-enrichment in ICE. The chemical and isotopic heterogeneities observed in the peridotites from the Charlie Gibbs TZ therefore document distinct histories of melt depletion and/or re-enrichment, as discussed further below.

'Secondary lherzolites' formed by melt-peridotite reaction

The low TiO_2, Zr and middle and heavy REE contents of the lherzolites require high degrees of melting of a depleted mantle (DM)-like peridotite[23] (12–14%), but their Na_2O and light REE contents are too high to be attributed to such extensive fractional melting (Fig. 2a,b), and thus result from melt-peridotite reaction. Nevertheless, the preservation of εHf up to 463 suggests that the peridotites have melted at least 1 Ga before renewed melting under the MAR (Extended Data Fig. 6).

The low εNd despite high εHf values of the lherzolites can therefore not be produced by partial melting alone, and show that they also reacted with migrating melts (for example, ref. 8) (Fig. 3a,b and see model details in Extended Data Figs. 4 and 5). In principle, both ancient (>0.2 Ga) and recent melt-rock reaction can account for the sharply decreasing Hf isotope ratios at low, MORB-like Nd isotope ratios of the lherzolites (Fig. 3). The abundant volcanism in the northern part of the Charlie Gibbs TZ is evidence for sustained melt production and relatively hot mantle[21], and it is therefore likely that the local peridotites have reacted with migrating melts during or following renewed partial melting under the MAR. In addition, such recent melt-rock reactions better agree with the low εNd of the least-depleted lherzolite sample[3] (Fig. 3b). Nevertheless, ancient melt-rock reaction cannot be ruled out, but must have been limited because the presence of high Hf isotope ratios implies that high Lu/Hf persisted for at least 1 Ga before recent melting (details provided in Methods).

In contrast to the lherzolites, the composition of the harzburgites is similar to residues of moderate degrees of fractional melting (7–10% according to the melting model shown in Extended Data Fig. 6) and limited reactions with melts under the present MAR. However, their Hf–Nd isotope ratios indicate a long-term evolution with moderate ICE depletion. Two samples have MORB-like Nd–Hf isotope ratios, falling within the range of basalts erupted at the Charlie Gibbs TZ[24], whereas two harzburgites have εNd and εHf much higher than any MORB erupted along the MAR. These εNd and εHf values indicate that the harzburgites have evolved with lower Lu/Hf and Sm/Nd than the associated lherzolites, either due to low degrees of ancient melting (melting degrees <3%, as shown in the melting trend in Fig. 3) or

https://doi.org/10.1038/s41561-024-01532-z

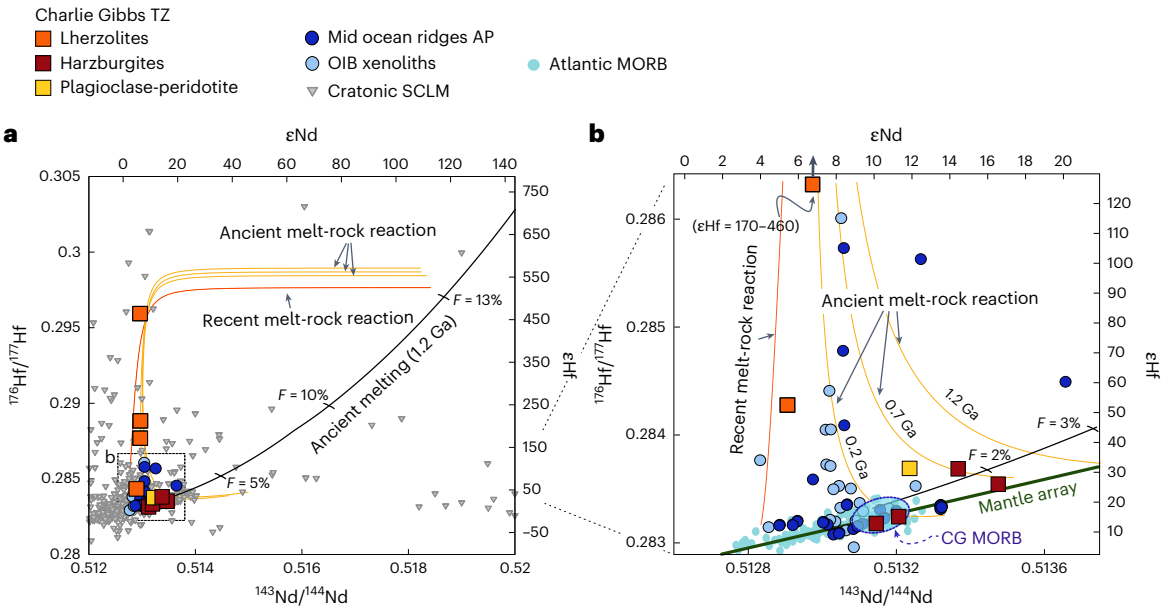

Fig. 3 | Effects of past and recent partial melting and melt-rock reaction on the Nd–Hf isotope ratios of mantle peridotites compared with the cpx in Charlie Gibbs peridotites. a, Present-day isotope ratios following ancient melt-rock interactions (1.2, 0.7 and 0.2 Ga, orange lines) of cpx from an ultradepleted ancient mantle residue (F = 13% melting at 1.2 Ga of DM[48]) compared with cpxs from Charlie Gibbs peridotites (error bars are smaller than the data points), global abyssal peridotites and cratonic SCLM peridotites (symbols as in Fig. 1). **b**, Close up of **a** showing the model results and MORB from Charlie Gibbs and MAR. Note that ancient and recent melt-rock reactions (indicated as orange and red lines, respectively) both shift the isotope ratios of the modified peridotites towards the Nd isotope ratios of the migrating melt. At low degrees of interaction, ancient and recent melt-rock reactions can both reproduce the Hf–Nd isotope ratios of most Charlie Gibbs lherzolites, starting from a common ultra-DM mantle protolith. Nonetheless, the recent melt-rock reaction best fits the low Nd isotope ratios of the lherzolites that also have the least radiogenic Hf isotope ratios (see text for further details). On the other hand, the MORB-like Hf–Nd isotope ratios of the residual harzburgites can be explained either by high degrees of ancient melt-rock reactions[3] or by low degrees of ancient partial melting (<3%) of a DM mantle. Details of the calculations of the melting and melt-rock reaction processes are given in Methods.

near-complete chemical resetting by an ancient melt-rock reaction[3]. In either scenario, the harzburgites were cpx- and ICE-rich peridotites before they re-melted extensively under the present-day MAR, and thereby acquired their residual, cpx- and ICE-depleted characteristics. Remarkably, however, these rocks did not react recently with migrating or stalled melts.

Links to the Iceland plume

At Iceland, extensive melting over the ridge-centred Iceland plume produces anomalously thick oceanic crust and exposes the MAR above sea level (Fig. 4a). Geodynamic models show that if a mantle plume rises under an active spreading centre, the upwelling mantle is channelled into the adjacent ridges and pushes the pre-existing asthenospheric mantle away. Although dependent on poorly constrained material properties of the Iceland plume, the consequence in these geodynamic models is that 'only plume material is present in the melting zone over the whole distance of the ridge influenced by the plume'[25]. Given that the Iceland plume has been active since ca. 55 Ma (refs. 19,20,26), any pre-existing asthenospheric mantle under the MAR adjacent to Iceland has long been flushed out. MORB and the associated oceanic lithosphere of the MAR adjacent to Iceland have therefore been generated by melting mantle derived exclusively from the Iceland plume[19,27,28].

The seismic velocity model in Fig. 4b,c (and refs. 17–20) shows that the low seismic velocities that delineate the Iceland plume extend to the northern part of the Charlie Gibbs TZ. The mantle Bouguer anomaly (MBA) shows a similar pattern (Fig. 4c). The MBA takes into account crustal thickness variations or density anomalies and is computed following methods detailed in ref. 29, incorporating available free air gravity data (Fig. 4c and Extended Data Fig. 1). MBA and seismic velocity patterns along the MAR overlap, suggesting that the Charlie Gibbs TZ is a major boundary between the upwelling Iceland plume and the mantle under the MAR to the south. The peridotites from the Charlie Gibbs TZ investigated here can therefore be considered samples of the predominant peridotite of the upwelling Iceland plume and, with the possible exception of peridotite xenoliths in Hawaiian lavas[30], they are the only direct peridotite samples of an active mantle plume.

The estimated minimum degree of ancient melt depletion (12–14%) of the lherzolites from the Charlie Gibbs TZ shows that ICE-depleted, buoyant peridotites are part of the Iceland plume. At pressures ranging from 3 to 6 GPa, corresponding to depths of ~100–200 km (Fig. 4c), this extent of prior melt depletion (12–14%) makes them ~1.5% lighter than fertile mantle compositions[31], which is equivalent to a temperature increase of ~200–300 °C (ref. 31). The low density of melt-depleted peridotite can therefore compensate for the negative buoyancy of recycled crust in the Iceland plume[32–35], and causes its positive thermochemical buoyancy, despite its moderate, yet still uncertain, excess temperature[36,37]. Notably, both the harzburgites and the lherzolites were already melt depleted before recent melting, and thus light and compositionally buoyant. Upwelling of a plume that is predominantly composed of such heterogeneous melt-depleted peridotite thus accounts for the heightened topography, increased melt production and formation of thick oceanic crust at Iceland and the adjacent MAR. Importantly, the ICE-depleted yet cpx-rich lherzolites from the Charlie Gibbs TZ show that such ancient, melt-depleted peridotites can also produce abundant melt[2–4,24].

Implications for the origin of V-shaped ridges

Variability in melt production with a periodicity of 5–10 Ma, associated with along-axis flow of the Icelandic plume, produces the diachronous V-shaped ridges of thick crust along the Reykjanes Ridge[26,38–41]. Pulses of increased melt production may be caused by temperature variations of the Iceland plume related to hot solitary waves triggered by thermal instabilities in the mantle[26,39,40] or viscous heating of high-viscosity blobs in the rising plume[26]. However, such temperature fluctuations of

https://doi.org/10.1038/s41561-024-01532-z

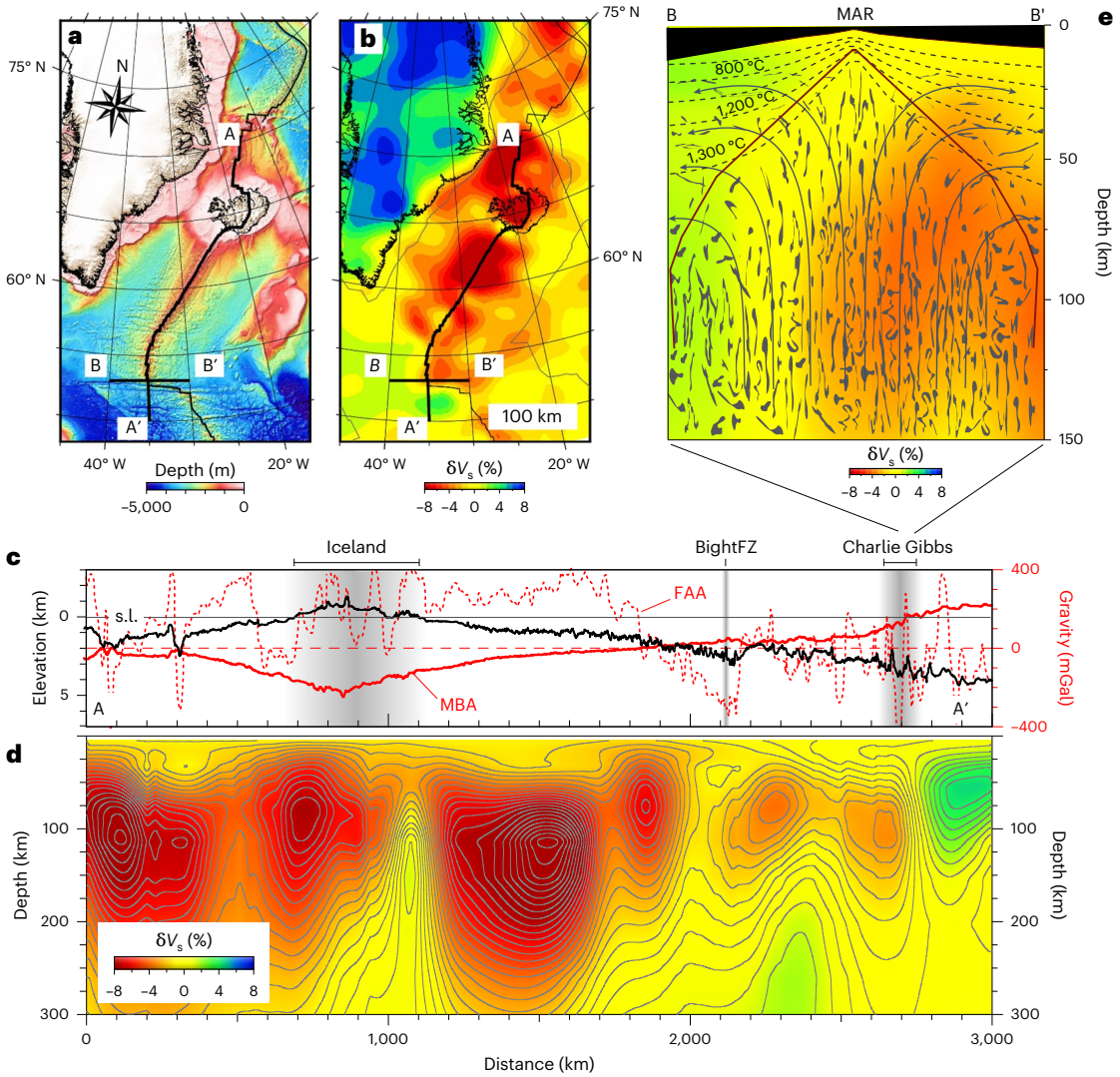

Fig. 4 | Bathymetry and waveform tomography model of the North Atlantic. **a**, A bathymetric map of the North Atlantic from the GEBCO 2023 Grid (https://doi.org/10.5285/f98b053b-0cbc-6c23-e053-6c86abc0af7b; GEBCO Compilation Group). **b**, Seismic tomography by the recent NAT2021 model calculated at 100 km depth. δV_s, shear wave velocity anomaly[29]. **c**,**d**, Bathymetry, free air (FAA) and MBA (**c**), and δV_s (**d**) along section A–A′ from **b**. Bight FZ, bight fracture zone; s.l., sea level. **e**, A schematic image of the melting region north of Charlie Gibbs (B–B′) including a crosscut section of δV_s. Enriched, fertile lithologies are widespread in the mantle, ranging from depleted to ultradepleted compositions. Low-velocity anomalies, $\delta V_s < 0$, may correspond to ultradepleted, buoyant mantle locally converted into lherzolite by interaction with migrating melts produced by enriched lithologies.

the Iceland plume may[42], or may not[37], be supported by mantle potential temperatures inferred from the crystallization temperatures of magmatic phenocrysts in Icelandic lavas.

Alternatively, intrinsic buoyancy variations due to variably depleted peridotitic domains, that is, the predominant component of the Iceland plume[32,35,43], may also lead to periods of increased plume flux and enhanced magma production[40,41]. Variations in the average extent of melt depletion of the predominant peridotite component along the rising Iceland plume appear likely, given the variable melt depletion of the peridotites from the Charlie Gibbs TZ. The variable extent of average melt depletion of peridotite results in density variations[44] that are similar to the small temperature fluctuations (several tens of °C) proposed for forming the V-shaped Reykjanes Ridge[26,39,45,46]. Note that the magma productivity of melt-depleted, yet still cpx-rich, peridotite is sufficient for increased melt production resulting from density-driven pulses of higher plume flux (see the discussion above and refs. 3,4,47,48). Hence, variable peridotite depletion along the rising plume may have triggered the pulses of enhanced plume flux and magma production required to generate the V-shaped Reykjanes Ridge.

Implications for MORB compositions along the Reykjanes Ridge

Bianco and co-workers[28] have shown that the flow and melting systematics of a compositionally and lithologically heterogeneous mantle along a plume-influenced ridge produces 'gradients in mantle dynamics and melting (that) cause along-axis geochemical variations', and 'transfers material that was partially depleted near the centre of the plume laterally along the axis'. Hence, melting close to the plume centre partly consumes fertile, enriched recycled components before the plume material moves further along axis, resulting in a gradual decrease of the compositional and isotopic 'plume signature' along the Reykjanes Ridge.

High $^3He/^4He$ values are retained in MORB along the entire Reykjanes Ridge, including the MAR segment immediately north of the Charlie Gibbs TZ[49]. This observation supports the geophysical constraints (discussed above) that mantle derived from the Iceland plume expands along the Reykjanes Ridge down to the Charlie Gibbs TZ at 53° N, and is consistent with the isotopic domain delineated by Sr–Nd–Hf–Pb isotope ratios in basalts from Iceland and adjacent ridges[50].

Moreover, Hf–Nd (and Sr–Pb) isotope ratios of MORB collected on a north–south transect across the Charlie Gibbs TZ also indicate that the fracture zone at 53° N represents a geochemical boundary: MORB in the northern segment of the fracture zone have higher $^{176}Hf/^{177}Hf$ at a given $^{143}Nd/^{144}Nd$ (Extended Data Fig. 7), and hence a higher contribution of melts from ICE-depleted peridotite[5,24,48,51,52], relative to MORB formed at the MAR to the south.

The variable contribution of melts from ICE-enriched components and variably ICE-depleted peridotite also explains much of the compositional variation of Icelandic basalts[32–35,53] as well as the differences between on- and off-rift Icelandic basalts. Icelandic basalts produced on axis have higher Hf (Nd) isotope ratios than basalts produced off axis, because the thinner lithosphere leads to higher degrees of melting and more effective dilution of melts from ICE-enriched components by melts from ICE-depleted peridotite[54].

In summary, the ultradepleted compositions of lherzolites from the Charlie Gibbs TZ suggests that a large part of the Iceland plume consists of ancient, ICE-depleted peridotites from which large extents of melts (12–14%) were extracted at least 1 Ga ago (Extended Data Figs. 5 and 6) before re-melting as part of the Iceland plume. These ultradepleted peridotites compensate for the excess density of recycled crust in the Iceland plume and cause its positive thermochemical buoyancy, despite its relatively moderate excess temperature. Although being melt depleted, these peridotites are still cpx rich (both before and after recent melting and melt-rock reaction), and can produce the thick Icelandic crust which, in combination with the low density of the peridotites, accounts for the elevated topography of the North Atlantic region. Variation in the average extent of peridotite depletion along the rising plume could lead to density-driven pulses of higher plume flux and thus to periods of high magma production that generate the V-shaped Reykjanes Ridge. Moreover, the geodynamics of melting a heterogeneous, ridge-centred plume that expands along the adjacent ridge axes[27,28] causes the continuous Icelandic isotopic province that extends from Iceland southward along the Reykjanes Ridge to the Charlie Gibbs TZ, and northward until Lena Trough[50].

Ancient and extensively melt-depleted peridotites similar to those found in Iceland may also dominate other major mantle upwellings, for example, those under Hawaii[30,55–57], the Azores[57] or the Canary Islands[58]. Variable peridotite depletion, and thus density fluctuations upstream of a rising plume, may therefore also lead to variable plume flux over other major hot spots, and affect the geometry of evolving mantle plumes[59,60]. So far, the compositional contribution to the thermochemical buoyancy of mantle plumes, and the mantle's convective motion in general, may therefore have been underestimated.

Online content

Any methods, additional references, Nature Portfolio reporting summaries, source data, extended data, supplementary information, acknowledgements, peer review information; details of author contributions and competing interests; and statements of data and code availability are available at https://doi.org/10.1038/s41561-024-01532-z.

References

1. Salters, V. J. M. & Zindler, A. Extreme $^{176}Hf/^{177}Hf$ in the sub-oceanic mantle. *Earth Planet. Sci. Lett.* **129**, 13–30 (1995).
2. Stracke, A. et al. Abyssal peridotite Hf isotopes identify extreme mantle depletion. *Earth Planet. Sci. Lett.* **308**, 359–368 (2011).
3. Sani, C., Sanfilippo, A., Peyve, A. A., Genske, F. & Stracke, A. Earth mantle's isotopic record of progressive chemical depletion. *AGU Adv.* **4**, e2022AV000792 (2023).
4. Byerly, B. L. & Lassiter, J. C. Isotopically ultradepleted domains in the convecting upper mantle: implications for MORB petrogenesis. *Geology* **42**, 203–206 (2014).
5. Sanfilippo, A., Salters, V., Tribuzio, R. & Zanetti, A. Role of ancient, ultra-depleted mantle in mid-ocean-ridge magmatism. *Earth Planet. Sci. Lett.* **511**, 89–98 (2019).
6. Tilhac, R., Begg, G. C., O'Reilly, S. Y. & Griffin, W. L. A global review of Hf-Nd isotopes: new perspectives on the chicken-and-egg problem of ancient mantle signatures. *Chem. Geol.* **609**, 121039 (2022).
7. Seyler, M., Lorand, J.-P., Toplis, M. J. & Godard, G. Asthenospheric metasomatism beneath the mid-ocean ridge: evidence from depleted abyssal peridotites. *Geology* **32**, 301–304 (2004).
8. Le Roux, V., Bodinier, J.-L., Alard, O., O'Reilly, S. Y. & Griffin, W. L. Isotopic decoupling during porous melt flow: a case-study in the Lherz peridotite. *Earth Planet. Sci. Lett.* **279**, 76–85 (2009).
9. Brunelli, D. & Seyler, M. Asthenospheric percolation of alkaline melts beneath the St. Paul region (Central Atlantic Ocean). *Earth Planet. Sci. Lett.* **289**, 393–405 (2010).
10. Warren, J. M. & Shimizu, N. Cryptic variations in abyssal peridotite compositions: evidence for shallow-level melt infiltration in the oceanic lithosphere. *J. Petrol.* **51**, 395–423 (2010).
11. Brunelli, D., Paganelli, E. & Seyler, M. Percolation of enriched melts during incremental open-system melting in the spinel field: a REE approach to abyssal peridotites from the Southwest Indian Ridge. *Geochim. Cosmochim. Acta* **127**, 190–203 (2014).
12. Warren, J. M. Global variations in abyssal peridotite compositions. *Lithos* **248–251**, 193–219 (2016).
13. Van den Bleeken, G., Muentener, O. & Ulmer, P. Reaction processes between tholeiitic melt and residual peridotite in the uppermost mantle: an experimental study at 0.8 GPa. *J. Petrol.* **51**, 153–183 (2010).
14. Borghini, G. et al. Fast REE re-distribution in mantle clinopyroxene via reactive melt infiltration. *Geochem. Perspect. Lett.* https://doi.org/10.7185/geochemlet.2323 (2023).
15. Zhou, H. & Dick, H. J. B. Thin crust as evidence for depleted mantle supporting the Marion Rise. *Nature* **494**, 195–200 (2013).
16. Schilling, J. G. Iceland mantle plume: geochemical study of Reykjanes Ridge. *Nature* **242**, 565–571 (1973).
17. Wolfe, C. J., Bjarnason, I. T., VanDecar, J. C. & Solomon, S. C. Seismic structure of the Iceland mantle plume. *Nature* **385**, 245–247 (1997).
18. French, S. W. & Romanowicz, B. Broad plumes rooted at the base of the Earth's mantle beneath major hotspots. *Nature* **525**, 95–99 (2015).
19. Steinberger, B., Bredow, E., Lebedev, S., Schaeffer, A. & Torsvik, T. Widespread volcanism in the Greenland–North Atlantic region explained by the Iceland plume. *Nat. Geosci.* **12**, 61–68 (2019).
20. Celli, N. L., Lebedev, S., Schaeffer, A. J. & Gaina, C. The tilted Iceland plume and its effect on the North Atlantic evolution and magmatism. *Earth Planet. Sci. Lett.* **569**, 117048 (2021).
21. Skolotnev, S. et al. Crustal accretion along the northern Mid Atlantic Ridge (52°–57° N): preliminary results from expedition V53 of R/V Akademik Sergey Vavilov. *Ofioliti* **48**, 13–30 (2023).
22. McDonough, W. F. & Sun, S.-S. The composition of the Earth. *Chem. Geol.* **120**, 223–253 (1995).
23. Salters, V. J. & Stracke, A. Composition of the depleted mantle. *Geochem. Geophys. Geosyst.* **5**, Q05B07 (2004).
24. Salters, V. J., Mallick, S., Hart, S. R., Langmuir, C. E. & Stracke, A. Domains of depleted mantle: new evidence from hafnium and neodymium isotopes. *Geochem. Geophys. Geosyst.* **12**, Q08001 (2011).
25. Ito, G., Lin, J. & Gable, C. Interaction of mantle plumes and migrating mid-ocean ridges: implications for the Galápagos plume-ridge system. *J. Geophys. Res.* **102**, 15403–15417 (1997).
26. Parnell-Turner, R. et al. A continuous 55-million-year record of transient mantle plume activity beneath Iceland. *Nat. Geosci.* **7**, 914–919 (2014).

27. Ito, G., Shen, Y., Hirth, G. & Wolfe, C. Mantle flow, melting, and dehydration of the Iceland mantle plume. *Earth Planet. Sci. Lett.* **165**, 81–96 (1999).
28. Bianco, T. D., Ito, G., van Hunen, J., Mahoney, J. J. & Ballmer, M. D. Geochemical variations at ridge-centered hotspots caused by variable melting of a veined mantle plume. *Earth Planet. Sci. Lett.* **371–372**, 191–202 (2013).
29. Ligi, M., Cuffaro, M., Muccini, F. & Bonatti, E. Generation and evolution of the oceanic lithosphere in the North Atlantic. *La Riv. del. Nuovo Cim.* **45**, 587–659 (2022).
30. Bizimis, M., Griselin, M., Lassiter, J. C., Salters, V. J. M. & Sen, G. Ancient recycled mantle lithosphere in the Hawaiian plume: osmium–hafnium isotopic evidence from peridotite mantle xenoliths. *Earth Planet. Sci. Lett.* **257**, 259–273 (2007).
31. Schutt, D. L. & Lesher, C. E. Effects of melt depletion on the density and seismic velocity of garnet and spinel lherzolite. *J. Geophys. Res. Solid Earth* https://doi.org/10.1029/2003JB002950 (2006).
32. Stracke, A., Zindler, A., Salters, V. J., McKenzie, D. & Grönvold, K. The dynamics of melting beneath Theistareykir, northern Iceland. *Geochem Geophys. Geosyst.* **4**, 8513 (2003).
33. Kokfelt, T. F. et al. Combined trace element and Pb–Nd–Sr–O isotope evidence for recycled oceanic crust (upper and lower) in the Iceland mantle plume. *J. Petrol.* **47**, 1705–1749 (2006).
34. Koornneef, J. M. et al. Melting of a two-component source beneath Iceland. *J. Petrol.* **53**, 127–157 (2012).
35. Shorttle, O., Maclennan, J. & Lambart, S. Quantifying lithological variability in the mantle. *Earth Planet. Sci. Lett.* **395**, 24–40 (2014).
36. Herzberg, C. & Asimow, P. PRIMELT3 MEGA.XLSM software for primary magma calculation: peridotite primary magma MgO contents from the liquidus to the solidus. *Geochem. Geophys. Geosyst.* **16**, 563–578 (2015).
37. Matthews, S., Wong, K., Shorttle, O., Edmonds, M. & Maclennan, J. Do olivine crystallization temperatures faithfully record mantle temperature variability? *Geochem. Geophys. Geosyst.* **22**, e2020GC009157 (2021).
38. Ito, G. et al. Seismic anisotropy and shear wave splitting associated with mantle plume–plate interaction. *J. Geophys. Res. Solid Earth* **119**, 4923–4937 (2014).
39. Jones, S. M. et al. A joint geochemical–geophysical record of time-dependent mantle convection south of Iceland. *Earth Planet. Sci. Lett.* **386**, 86–97 (2014).
40. Martinez, F. & Hey, R. Propagating buoyant mantle upwelling on the Reykjanes Ridge. *Earth Planet. Sci. Lett.* **457**, 10–22 (2017).
41. Zha, C., Lin, J., Zhou, Z., Xu, M. & Zhang, X. Effects of hotspot-induced long-wavelength mantle melting variations on magmatic segmentation at the Reykjanes Ridge: insights from 3D geodynamic modeling. *J. Geophys. Res. Solid Earth* **127**, e2021JB023244 (2022).
42. Spice, H. E., Fitton, J. G. & Kirstein, L. A. Temperature fluctuation of the Iceland mantle plume through time. *Geochem. Geophys. Geosyst.* **17**, 243–254 (2016).
43. Brown, E. L. & Lesher, C. E. North Atlantic magmatism controlled by temperature, mantle composition and buoyancy. *Nat. Geosci.* **7**, 820–824 (2014).
44. Afonso, J. C. & Schutt, D. L. The effects of polybaric partial melting on density and seismic velocities of mantle restites. *Lithos* **134–135**, 289–303 (2012).
45. White, R. S., Bown, J. & Smallwood, J. R. The temperature of the Iceland plume and origin of outward-propagating V-shaped ridges. *J. Geol. Soc.* **152**, 1039–1045 (1995).
46. Poore, H., White, N. & Maclennan, J. Ocean circulation and mantle melting controlled by radial flow of hot pulses in the Iceland plume. *Nat. Geosci.* **4**, 558–561 (2011).
47. Sani, C. et al. Ultra-depleted melt refertilization of mantle peridotites in a large intra-transform domain (Doldrums Fracture Zone; 7–8° N, Mid-Atlantic Ridge). *Lithos* **374–375**, 105698 (2020).
48. Sanfilippo, A., Salters, V. J., Sokolov, S. Y., Peyve, A. A. & Stracke, A. Ancient refractory asthenosphere revealed by mantle re-melting at the Arctic Mid Atlantic Ridge. *Earth Planet. Sci. Lett.* **566**, 116981 (2021).
49. Hilton, D. R., Thirlwall, M. F., Taylor, R. N., Murton, B. J. & Nichols, A. Controls on magmatic degassing along the Reykjanes Ridge with implications for the helium paradox. *Earth Planet. Sci. Lett.* **183**, 43–50 (2000).
50. Stracke, A., Willig, M., Genske, F., Béguelin, P. & Todd, E. Chemical geodynamics insights from a machine learning approach. *Geochem. Geophys. Geosyst.* **23**, e2022GC010606 (2022).
51. Willig, M., Stracke, A., Beier, C. & Salters, V. J. M. Constraints on mantle evolution from Ce–Nd–Hf isotope systematics. *Geochim. Cosmochim. Acta* **272**, 36–53 (2020).
52. Sani, C. et al. Sampling Earth's mantle at intra-transform spreading ridges. *Geochim. Cosmochim. Acta* **374**, 156–172 (2024).
53. Maclennan, J. et al. Melt mixing and crystallization under Theistareykir, northeast Iceland. *Geochem. Geophys. Geosyst.* **4**, 8624 (2003).
54. Harðardóttir, S., Matthews, S., Halldórsson, S. A. & Jackson, M. G. Spatial distribution and geochemical characterization of Icelandic mantle end-members: Implications for plume geometry and melting processes. *Chem. Geol.* **604**, 120930 (2022).
55. Lassiter, J. C. & Hauri, E. H. Osmium-isotope variations in Hawaiian lavas: evidence for recycled oceanic lithosphere in the Hawaiian plume. *Earth Planet. Sci. Lett.* **164**, 483–496 (1998).
56. DeFelice, C., Mallick, S., Saal, A. E. & Huang, S. An isotopically depleted lower mantle component is intrinsic to the Hawaiian mantle plume. *Nat. Geosci.* **12**, 487–192, (2019).
57. Stracke, A., Genske, F., Berndt, J. & Koornneef, J. M. Ubiquitous ultra-depleted domains in Earth's mantle. *Nat. Geosci.* **12**, 851–855 (2019).
58. Day, J. M. D., Pearson, D. G., Macpherson, C. G., Lowry, D. & Carracedo, J. C. Evidence for distinct proportions of subducted oceanic crust and lithosphere in HIMU-type mantle beneath El Hierro and La Palma, Canary Islands. *Geochim. Cosmochim. Acta* **74**, 6565–6589 (2010).
59. Kumagai, I., Davaille, A., Kurita, K. & Stutzmann, E. Mantle plumes: thin, fat, successful, or failing? Constraints to explain hot spot volcanism through time and space. *Geophys. Res. Lett.* **35**, L16301 (2008).
60. Adam, C., Caddick, M. J. & King, S. D. Pyroxenite causes fat plumes and stagnant slabs. *Geophys. Res. Lett.* **44**, 4730–4737 (2017).

Methods

Charlie Gibbs peridotites and basalt glasses

The Charlie Gibbs TZ is located in the North Atlantic between 52° and 53° N where it displaces the MAR for about 380 km. The TZ is located along a segment of the mid-ocean ridge immediately south of the Reykjanes Ridge. The Charlie Gibbs TZ is composed of two parallel transform faults, subdivided by a short intra-transform ridge segment. All samples in this study were collected during expeditions S50 and V53 in October 2020 and October 2021[21]. Basalt glasses were sampled at different locations along the southern and northern segments of the MAR, including the intra-transform spreading centre, whereas mantle peridotites were collected exclusively along the northern transform (see sample locations in Extended Data Fig. 1). The sample locations, mineralogy and textural features are reported in Supplementary Table 1 for peridotites and Supplementary Table 4 for basalt glasses. Details on peridotite textures are also reported in Extended Data Fig. 3. Harzburgites are serpentinized, brownish to black and are generally pyroxene poor. They have large, partly deformed orthopyroxene and subrounded spinel within a serpentinized olivine matrix. Cpx is mainly found as neoblasts surrounding porphyroclastic pyroxene. One sample contains a submillimetre plagioclase vein crosscutting the deformed mantle minerals. Lherzolites are partly weathered, brownish and commonly show a tectonite fabric. Large pyroxene and altered olivine are mantled by neoblastic pyroxenes. Spinel occurs as elongated irregular grains, often associated with fine-grained cpx. The lherzolite that has cpx with high-middle REE contents is characterized by the occurrence of random pyroxene-rich patches within the olivine-rich matrix.

Major and trace element concentrations

Four to six representative olivine, spinel and cpx grains and three basalt glass shards were selected for each peridotite and basalt sample, respectively. Major element concentrations were measured by electron probe microanalysis with a JEOL JXA8200 Superprobe at the Department of Earth Science Ardito Desio of Milano University using an accelerating voltage of 15 kV and a beam current of 15 nA. The trace element concentrations of cpx and basalt glasses were analysed on the same grains previously analysed for the major element compositions by laser ablation inductively coupled plasma mass spectrometry (ICP–MS) using a Triple Quadrupole ICP–MS Agilent Series 8900 interfaced to a GeoLas 193 nm excimer ablation system (Lambda Physik) at the Istituto di Geoscienze e Georisorse del Consiglio Nazionale delle Ricerche S.S. of Pavia. The ablation system was operated at a 10 Hz repetition rate, 50 µm spot size, with a fluence of about 9 J cm^{-2}. Helium was used as carrier gas and mixed with Ar downstream of the ablation cell. The NIST SRM 610 synthetic glass was used as external standard, with ^{44}Ca as internal standard[61]. Background and signal were measured for about 60 s, and the raw data were processed with the software package GLITTER. The precision and accuracy were assessed by repeated analyses of the BRC-2g reference material and were both generally better than ±10%. Major and trace element mineral compositions are reported in Supplementary Tables 2 and 3 for peridotites and Supplementary Table 4 for basalt glasses.

Neodymium and hafnium isotope ratios

The Hf and Nd isotope ratio measurements of cpxs and basalt glasses were performed at the Institut für Mineralogie, Universität Münster (Supplementary Tables 3 and 4). All sample materials (~150 mg, cpx and basalt glasses were hand-picked under a binocular microscope) were leached with H_2O_2 in an ultrasonic bath for about 2 h to remove Mn oxide coatings. Subsequently, the cpx were leached in 6 N HCl for about 2 h in an ultrasonic bath, followed by leaching in 6 N HCl for about 2 h at 100 °C to remove the effects of seawater alteration. The grains were dissolved in concentrated HF–HNO_3 (4:1) for 3 days at 140 °C. After drying at 120 °C, the samples were re-dissolved with 6 N HCl together with H_3BO_3 at 120 °C for 1 h and finally dried at 120 °C, before redissolving for ion exchange chromatography. Strontium and the high field strength and REE fractions of the samples were separated using standard cation exchange chromatography (Bio-Rad, AG50W-X8, mesh size 200–400 µm). Hafnium was purified from the high field strength fraction using Eichrom Ln Spec columns[62]. Neodymium was further purified from the REE fraction in a second column using Eichrom Ln Spec resin (mesh size 50–100 µm)[63]. The Nd and Hf isotope ratios were determined on a Thermo Scientific NEPTUNE Plus multi-collector ICP–MS at the University of Münster. Repeated measurements of the JMC-475 Hf standard gave an average $^{176}Hf/^{177}Hf$ of 0.282155 ± 16 (2 s.d., n = 12, determined on 10 ppb solutions). All Hf isotope ratios are reported relative to $^{176}Hf/^{177}Hf$ of 0.282160 (ref. 64). To verify the reproducibility of the isotope ratio analyses, small aliquots (that is, 5–10 mg) of the United States Geological Survey rock reference materials BHVO-2 and BCR-2 and BIR-1 were processed as unknowns and gave $^{176}Hf/^{177}Hf$ of 0.283092 ± 12 (2 s.d., n = 4) for BHVO-2, $^{176}Hf/^{177}Hf$ of 0.282856 ± 6 (2 s.d., n = 4) for BCR-2 and $^{176}Hf/^{177}Hf$ of 0.283282 ± 19 (2 s.d., n = 1) for BIR-1; all reference materials were diluted to about 4–8 ppb Hf to match typical concentrations of the sample solutions (Supplementary Table 3). Note that total procedural blanks were typically <10 pg of Hf, whereas the cpx samples yielded between 400 and 2,700 pg of Hf. The JNdi-1 (20 ppb) Nd bracketing standard was determined at $^{143}Nd/^{144}Nd$ of 0.512081 ± 12 (2 s.d., n = 17), and all data are normalized to JNdi-1 $^{143}Nd/^{144}Nd$ of 0.512115 (ref. 65). The United States Geological Survey rock standards are measured with $^{143}Nd/^{144}Nd$ of 0.512975 ± 15 (2 s.d., n = 4) for BHVO-2, with $^{143}Nd/^{144}Nd$ of 0.512634 ± 8 (2 s.d., n = 4) for BCR-2 and $^{143}Nd/^{144}Nd$ of 0.513099 ± 8 (2 s.d., n = 4) for BIR-1.

Geochemical modelling

Mantle melting. We reproduce the trace element and isotopic compositions of mantle residues using a dynamic melting model with fixed residual porosity (at 1%) and percentage of melting per km at 0.15% (ref. 3). The initial peridotite composition is the DM and partition coefficients from ref. 48. Melting begins at 100 km in the garnet-stability field until the total degree of melting reaches F = 3%, followed by further melting in the spinel stability field starting at 75 km. Melting reactions are recalculated at 60 km, 48 km, 33 km and 24 km. The present-day isotopic composition of ancient residues is calculated using initial isotope ratios at the time of melting according to a two-stage DM mantle evolution starting from primitive mantle at 3.5 Ga and present-day isotope ratios of $^{176}Hf/^{177}Hf$ of 0.28330 and $^{143}Nd/^{144}Nd$ of 0.51311 (ref. 48). Parameters and results are provided in Supplementary Table 5.

Melt-rock reaction. The melt-rock reaction model reproduces melt migrating through a peridotite column, modified by partial assimilation of peridotite and crystallization of new mineral phases. The trace element composition of the reacting melt and resulting peridotite is simulated using the non-dimensional plate model by ref. 66. The melt-rock reaction causes dissolution of olivine and crystallization of new cpx, following the mineralogical compositions of the peridotites from the Charlie Gibbs TZ. The incoming melt is assumed to crystallize in the matrix, neglecting mixing enthalpy and density differences, and the ICE and isotope contents are redistributed in chemical equilibrium between melt and solid. The starting peridotite is assumed to represent a residual peridotite (DM) after F = 13% (see melting model) composed of 78% olivine + 20% orthopyroxene + 2% cpx. The initial porosity is set at 1% and porosity, melt-rock ratio and the modal composition of the crystallizing cpx varies during the reaction. The starting mantle is designed as a column divided in 40 cells, where each cell represents a process increment for a total of 40 process increments[66]. The assimilation rate of peridotite minerals is set to 2‰ throughout the column and crystallization at 2% of the incremental melt fraction to assure a ratio of mass assimilated (M_a) to mass crystallized (M_c) of 0.99; the latter is

calculated using the following equation, where F is the dissolution rate and f is the crystallization rate:

$$\frac{M_a}{M_c} = \frac{(1-\varnothing)F}{(1-f)[\varnothing + F(1-\varnothing)]}$$

The results are reported in Extended Data Figs. 3 and 4 as REE–Hf composition of cpx in equilibrium with the migrating and reacting melt and the mass of crystallized cpx at each simulated increment. The parameters and results are provided in Supplementary Table 6.

The isotopic evolution during the melt-rock reaction process is calculated using an assimilation–fractional crystallization process using equations given in ref. 67. As starting melt for both the recent and ancient melt-rock reaction model, we used a MORB with εNd of 5 and εHf of 10 to account for the low Nd isotope of the lherzolite, with REE–Hf composition of a typical MORB[68]. The composition of the reacted peridotite is calculated at 1% increments, which indicate the mass fraction of peridotite equilibrated with the melt undergoing assimilation–fractional crystallization (scaled from 0% to 100%). The degree of interaction correspond to the 'F' in the equation in ref. 67. The initial isotopic ratios, calculated from Equation 15a in ref. 67, were added to the radiogenic ^{143}Nd and ^{176}Hf ingrowth based on the ^{147}Sm/^{144}Nd and ^{176}Lu/^{177}Hf ratios of the reacted peridotite. Three scenarios of melt rock reaction processes were calculated at 1.2, 0.7, 0.2 and 0 Ga. The parameters and results are provided in Supplementary Table 6.

Data availability

Geochemical data used in this paper are provided in Figshare at https://doi.org/10.6084/m9.figshare.24619665 (ref. 69). The results of the geochemical modelling are available as Supplementary Information.

References

61. Pearce, N. J. et al. A compilation of new and published major and trace element data for NIST SRM 610 and NIST SRM 612 glass reference materials. *Geostand. Newsl.* **21**, 115–144 (1997).
62. Münker, C., Weyer, S., Scherer, E. & Mezger, K. Separation of high field strength elements (Nb, Ta, Zr, Hf) and Lu from rock samples for MC–ICP–MS measurements. *Geochem., Geophys. Geosyst.* https://doi.org/10.1029/2001GC000183 (2001).
63. Pin, C. & Zalduegui, J. F. S. Sequential separation of light rare-earth elements, thorium and uranium by miniaturized extraction chromatography: application to isotopic analyses of silicate rocks. *Anal. Chim. Acta* **339**, 79–89 (1997).
64. Blichert-Toft, J., Chauvel, C. & Albarède, F. Separation of Hf and Lu for high-precision isotope analysis of rock samples by magnetic sector-multiple collector ICP–MS. *Contrib. Mineral. Petrol.* **127**, 248–260 (1997).
65. Tanaka, T. et al. JNdi-1: a neodymium isotopic reference in consistency with LaJolla neodymium. *Chem. Geol.* **168**, 279–281 (2000).
66. Vernières, J., Godard, M. & Bodinier, J. L. A plate model for the simulation of trace element fractionation during partial melting and magma transport in the Earth's upper mantle. *J. Geophys. Res. Solid Earth* **102**, 24771–24784 (1997).
67. DePaolo, D. J. Trace element and isotopic effects of combined wallrock assimilation and fractional crystallization. *Earth Planet. Sci. Lett.* **53**, 189–202 (1981).
68. Gale, A., Dalton, C. A., Langmuir, C. H., Su, Y. & Schilling, J. G. The mean composition of ocean ridge basalts. *Geochem. Geophys. Geosyst.* **14**, 489–518 (2013).
69. Sanfilippo, A. Major, trace elements and Nd–Hf isotope compositions of peridotites and associated MORB from the Charlie Gibbs Transform. *Figshare* https://doi.org/10.6084/m9.figshare.24619665 (2024).
70. Sandwell, D. T., Müller, R. D., Smith, W. H., Garcia, E. & Francis, R. New global marine gravity model from CryoSat-2 and Jason-1 reveals buried tectonic structure. *Science* **346**, 65–67 (2014).
71. Skolotnev, S. et al. *Seafloor Spreading and Tectonics at the Charlie Gibbs Transform System (52–53° N, Mid Atlantic Ridge): Preliminary Results from R/V AN Strakhov Expedition S50* (Ofioliti, 2021).

Acknowledgements

We thank A. Nazarevskiy and officers and crew of R/V Akademik Nikolaj Strakhov, and V. V. Beluga and officers and crew of R/V Akademik Sergey Vavilov. This study was supported by Accordo Bilaterale CNR/RFBR 2018-2020 (project no. CUP-B36C17000250005) and by the Italian Programma di Rilevante Interesse Nazionale (project nos. PRIN_2017KY5ZX8 to M.L. and PRIN_2022PC9NME to A. Sanfilippo), by the Deutsche Forschungs Gemeinschaft grant STR853/14-1 to A. Stracke and by the Russian Foundation for the Basic Research (project no. 18-55-7806 Ital_t) and the Russian Basic Research Program (project nos. FMUN-2019-0076, FMWE-2021-0005 and FMMG-2022-0003) to A.A.P.

Author contributions

A. Sanfilippo and A. Stracke conceived the idea and wrote the text. M.L. and M.C. developed the geophysical models and prepared Fig. 4. A.A.P. and M.L. provided funding and organized the expeditions. A. Sanfilippo and C.F. performed the geochemical models. S.S., C.F., V.B., D.B. and G.B. performed the preliminary petrological and geochemical study of the peridotites. S.S. and F.G. performed the isotope measurements.

Funding

Open access funding provided by Westfälische Wilhelms-Universität Münster.

Competing interests

The authors declare no competing interests.

Additional information

Extended data is available for this paper at https://doi.org/10.1038/s41561-024-01532-z.

Supplementary information The online version contains supplementary material available at https://doi.org/10.1038/s41561-024-01532-z.

Correspondence and requests for materials should be addressed to A. Sanfilippo or A. Stracke.

Peer review information *Nature Geoscience* thanks Sæmundur Halldórsson, Sarah Lambart and the other, anonymous, reviewer(s) for their contribution to the peer review of this work. Primary Handling Editor: Alison Hunt, in collaboration with the *Nature Geoscience* team.

https://doi.org/10.1038/s41561-024-01532-z

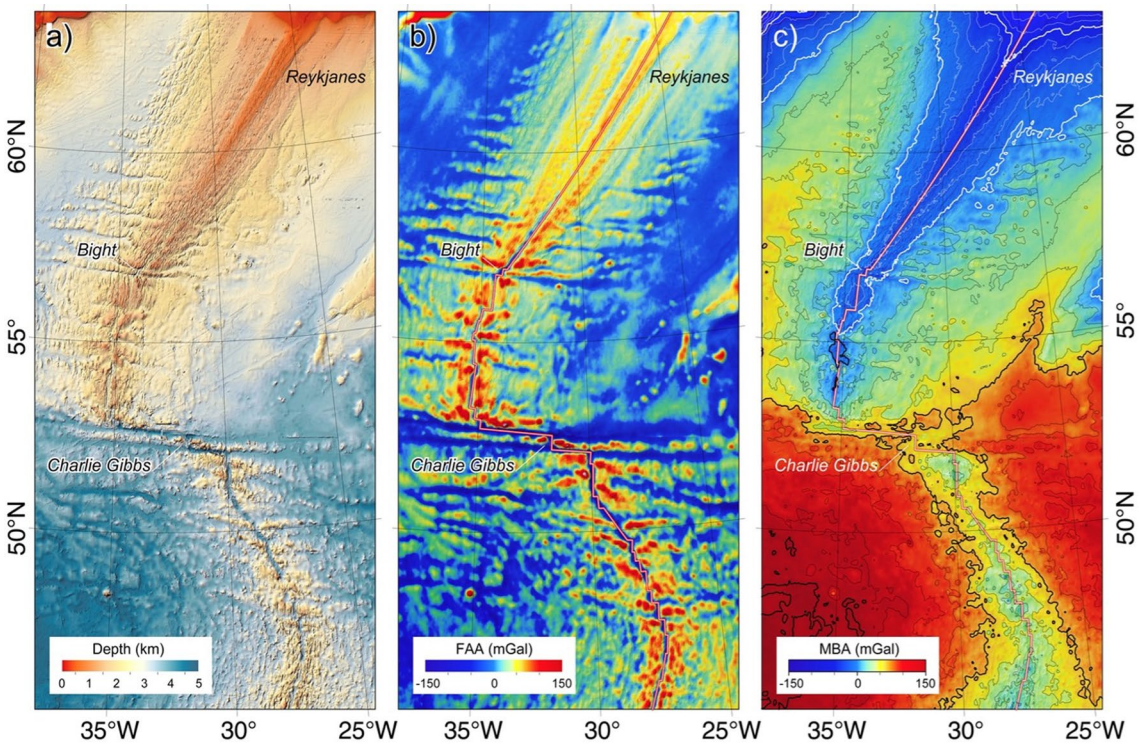

Extended Data Fig. 1 | Detail of variations in bathymetry (a), free-air gravity anomaly (b) and mantle Bouguer anomaly (c) of Mid Atlantic Ridge across Charlie Gibbs area. Bathymetry is from the GEBCO 2023 Grid (doi:10.5285/f98b053b-0cbc-6c23-e053-6c86abc0af7b; GEBCO Compilation Group), and free air gravity data are from the satellite derived gravity grid (version 32) of ref. 70. Variations of crustal thickness and upper mantle density anomalies affect the mantle Bouguer reduced gravity field. Their contribution has been evaluated following ref. 29 by evaluating the density contrast between water, crustal and mantle rocks, and the density variations in the mantle due to the temperature field. The mantle Bouguer correction (MBA) is obtained considering a water layer of density equal to 1040 kg/m^3, an 8 km constant thickness crust of density equal to 2690 kg/m^3, and a layer of mantle material of density equal to 3330 kg/m^3. The arbitrary zero level corresponds to the center of the range in anomaly amplitudes.

https://doi.org/10.1038/s41561-024-01532-z

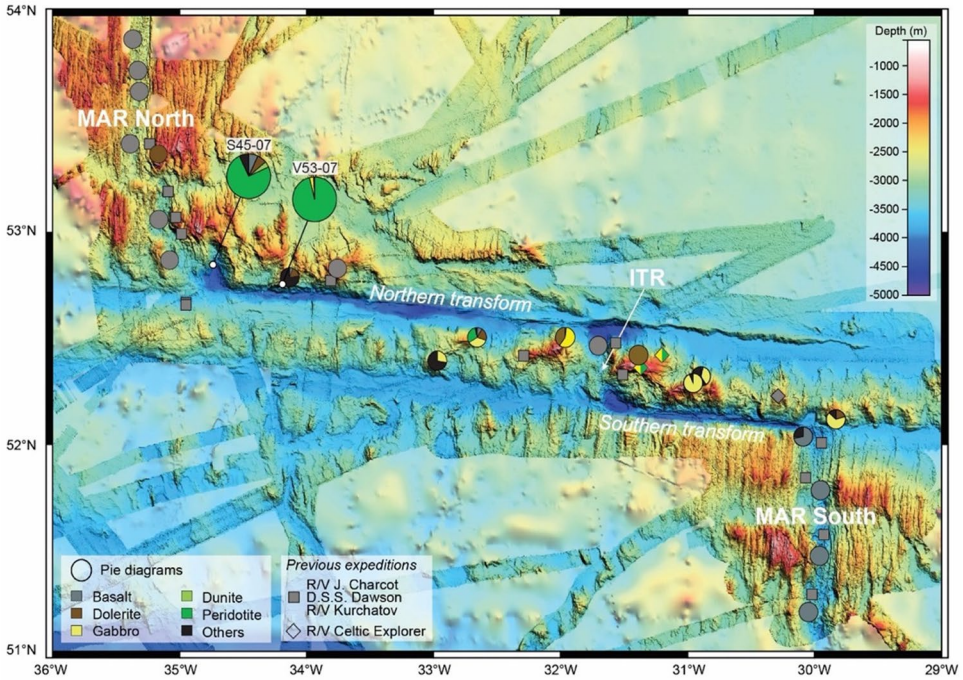

Extended Data Fig. 2 | Bathymetric map and dredge location within the Charlie Gibbs Transform Zone. Shaded relief image of the Charlie Gibbs Fracture zone obtained from the original swath bathymetry data acquired during the S50 and V53 expeditions (see[21,71]). Mantle peridotites were selected exclusively at the norther wall of the transform zone, whereas basalt glasses were sampled at different locations along the Mid Atlantic Ridge and in the intra-transform ridge segment (see Supplementary Tables 1 and 4).

https://doi.org/10.1038/s41561-024-01532-z

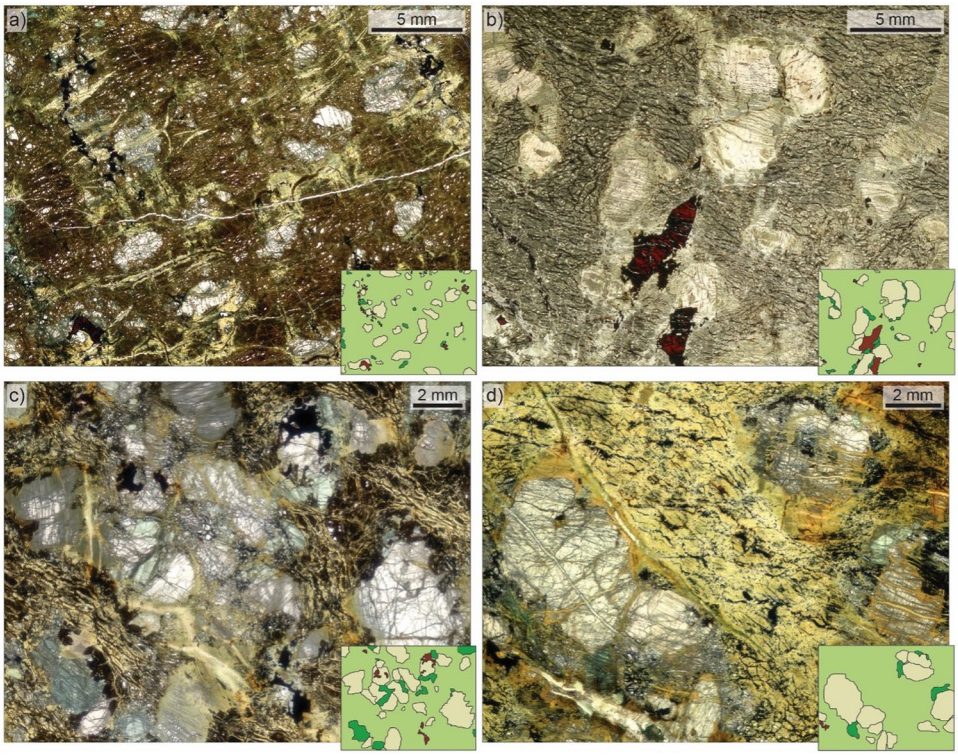

Extended Data Fig. 3 | Representative photomicrographs of the Charlie Gibbs peridotites. Insets in the bottom right corner give a representative view of the sample modal composition: olivine is shown in light green, orthopyroxene in beige, clinopyroxene in dark green and spinel in dark brown; **a**) Lherzolite V53-7-1, showing strong alteration of olivine but preserves the porphyroclastic texture of orthopyroxene, clinopyroxene and spinel; **b**) Lherzolite V53-7-4, showing large spinel crystals oriented parallel to the foliation defined by orthopyroxene elongation. Clinopyroxene occurs mostly at the contact between orthopyroxene porphyroclasts and olivine; **c**) Plagioclase harzburgite V53-7-14, showing an aggregate of large subequant orthopyroxenes and interstitial clinopyroxenes; **d**) Harzburgite V53-7-21, showing a porphyroclastic texture with the occurrence of coarse-grained orthopyroxene and interstitial clinopyroxene.

https://doi.org/10.1038/s41561-024-01532-z

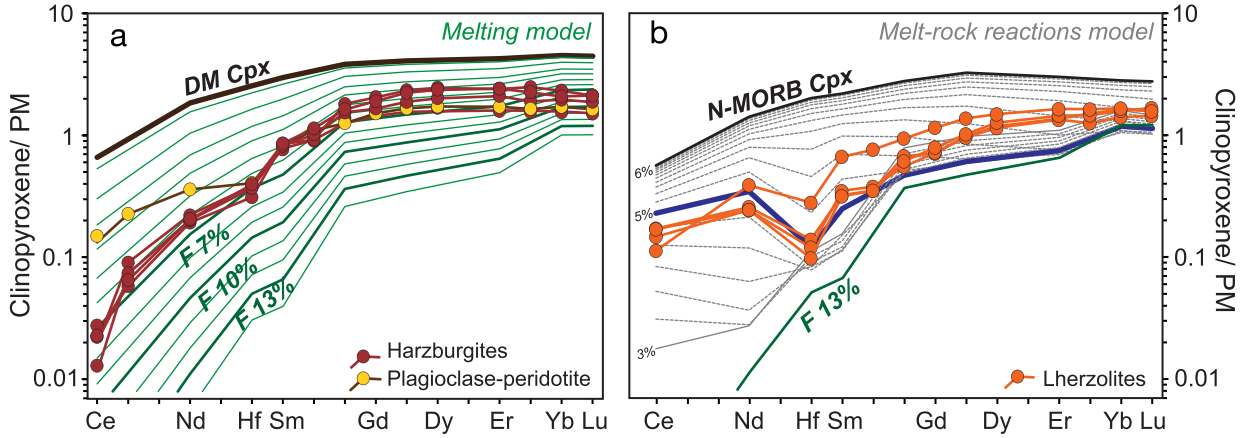

Extended Data Fig. 4 | Primitive Mantle-normalized Hf-Y-REE compositions of the Charlie Gibbs peridotites compared to the results of the melting (a) and melt-rock (b) reaction models. The natural samples are compared to clinopyroxene residual from different melting of spinel fractional melting (**a**) and melt-rock reaction processes (**b**). The REE compositions of the harzburgites are overall compatible with residues of partial melting at F = 7%. The trace elements composition of Pl-harzburgite is not comparable with melting trends, having higher LREE than pure melting residue. On the other hand, the middle REE and Hf contents of the clinopyroxene in the lherzolites require high melting degrees (13%) followed by low extents of melt-rock reaction (details of the melting and melt-rock reaction model in the Methods) between a residual harzburgite and a N-MORB. The reaction simulates assimilation and concomitant fractional crystallization, leading to progressive increase in clinopyroxene modal composition (in italic on plate b) as the reaction proceeds, from <3% modal clinopyroxene at low extents of melt-rock re-equilibration to ~6% at near complete re-equilibration of the harzburgite with the percolating melt. The best fit of REE-Hf composition of the lherzolites is obtained when clinopyroxene reaches ~5 wt% (see details in the Methods), consistent with petrographic observations.

https://doi.org/10.1038/s41561-024-01532-z

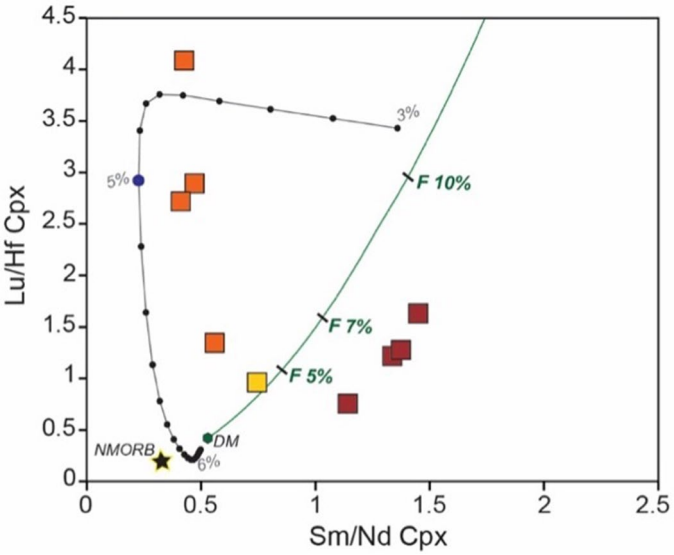

Extended Data Fig. 5 | Sm/Nd vs Lu/Hf ratio of the clinopyroxenes from the Charlie Gibbs peridotites. The samples are compared to clinopyroxene resulting from melting (at 5, 7 and 10 % melting degree; green line), and melt-rock reaction trend. The melt-rock reaction trend (grey line) is plotted as clinopyroxenes in equilibrium with the reacting and modified melt; each black dot indicates a single reaction increment corresponding to progressive decrease in olivine modal contents and concomitant increase in clinopyroxene modes (indicated in italic numbers). The modelled clinopyroxene modal contents reported for single increments in this plot correspond to those in Extended Data Fig. 2b. The composition of the reacting melt is also reported as a black star. Radiogenic Hf ingrowth following ancient melting and melt-rock reaction processes explain the trends in Fig. 3 of the main text.

https://doi.org/10.1038/s41561-024-01532-z

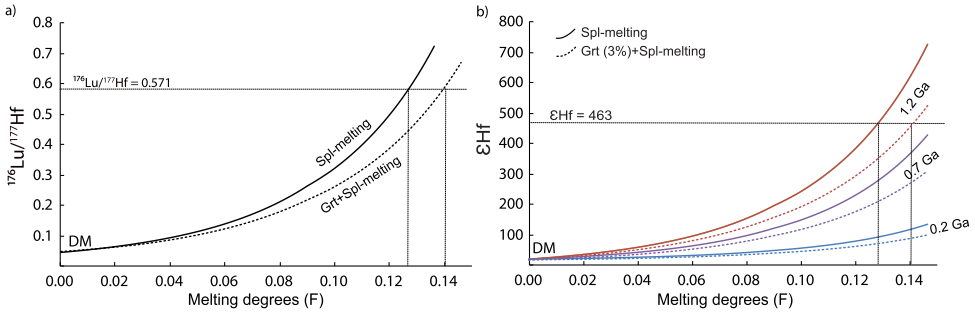

Extended Data Fig. 6 | Isotopic evolution of a residual peridotite created 1.2 Ga, 0.7 Ga and 0.2 Ga ago by variable degrees of partial melting. The model shows melting processes started in the garnet stability field (dashed lines) and spinel stability field (bold line) following the dynamic melting model explained in Material and Methods. Panel **a** shows the variation in $^{176}Lu/^{177}Hf$ versus melting degrees; panel **b** shows the isotopic evolution following radiogenic ingrowth at different times as indicated by the numbers on each trend. The $^{176}Lu/^{177}Hf$ and $^{176}Hf/^{177}Hf$ ratios of the clinopyroxene in the most depleted Charlie Gibbs lherzolite are plotted for comparison, and indicate that the high Hf isotopic ratio must be acquired following melting degrees of 12–14% at an age > 1Ga.

https://doi.org/10.1038/s41561-024-01532-z

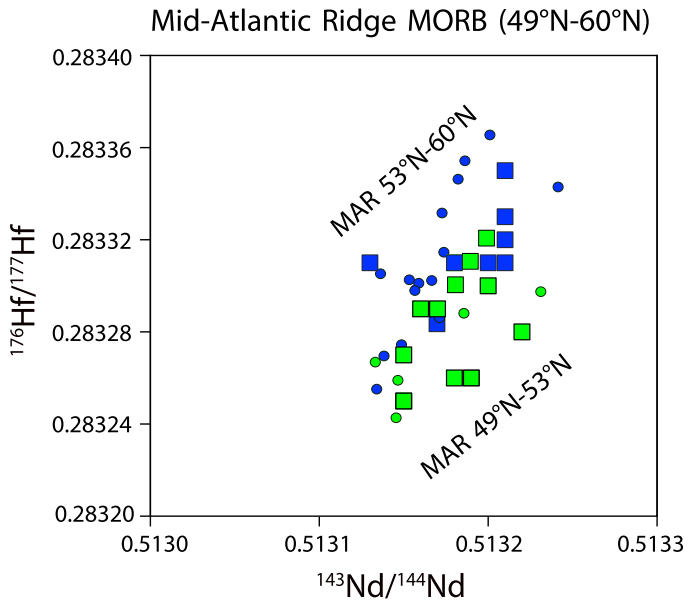

Extended Data Fig. 7 | Hf-Nd isotope variations of MORB glasses in the vicinity of the Charlie Gibbs Transform Zone. Sampling stations in Extended Data Fig. 2; major, trace elements and Nd-Hf isotope compositions in Supplementary Table 4. MORB North and South of Charlie Gibbs are represented in blue and green squares, respectively. Also shown are literature data of Atlantic MORB from MAR 49°-53°N (green circles) and 53° to 60°N (blue circles) (data source PetDB).